JOURNAL OF GEOPHYSICAL RESEARCH, VOL. 112, D12S04, doi:10.1029/2006JD007664, 2007



# Reactive nitrogen distribution and partitioning in the North American troposphere and lowermost stratosphere

H. B. Singh,[1] L. Salas,[1] D. Herlth,[1] R. Kolyer,[1] E. Czech,[1] M. Avery,[2] J. H. Crawford,[2] R. B. Pierce,[2] G. W. Sachse,[2] D. R. Blake,[3] R. C. Cohen,[4] T. H. Bertram,[4] A. Perring,[4] P. J. Wooldridge,[4] J. Dibb,[5] G. Huey,[6] R. C. Hudman,[7] S. Turquety,[7] L. K. Emmons,[8] F. Flocke,[8] Y. Tang,[9] G. R. Carmichael,[9] and L. W. Horowitz[10]

Received 15 June 2006; revised 21 November 2006; accepted 7 December 2006; published 4 April 2007.

[1] A comprehensive group of reactive nitrogen species (NO, $NO_2$, $HNO_3$, $HO_2NO_2$, PANs, alkyl nitrates, and aerosol-$NO_3^-$) were measured over North America during July/August 2004 from the NASA DC-8 platform (0.1–12 km). Nitrogen containing tracers of biomass combustion (HCN and $CH_3CN$) were also measured along with a host of other gaseous (CO, VOC, OVOC, halocarbon) and aerosol tracers. Clean background air as well as air with influences from biogenic emissions, anthropogenic pollution, biomass combustion, convection, lightning, and the stratosphere was sampled over the continental United States, the Atlantic, and the Pacific. The North American upper troposphere (UT) was found to be greatly influenced by both lightning $NO_x$ and surface pollution lofted via convection and contained elevated concentrations of PAN, ozone, hydrocarbons, and $NO_x$. Observational data suggest that lightning was a far greater contributor to $NO_x$ in the UT than previously believed. PAN provided a dominant reservoir of reactive nitrogen in the UT while nitric acid dominated in the lower troposphere (LT). Peroxynitric acid ($HO_2NO_2$) was present in sizable concentrations peaking at around 8 km. Aerosol nitrate appeared to be mostly contained in large soil based particles in the LT. Plumes from Alaskan fires contained large amounts of PAN and aerosol nitrate but little enhancement in ozone. A comparison of observed data with simulations from four 3-D models shows significant differences between observations and models as well as among models. We investigate the partitioning and interplay of the reactive nitrogen species within characteristic air masses and further examine their role in ozone formation.

**Citation:** Singh, H. B., et al. (2007), Reactive nitrogen distribution and partitioning in the North American troposphere and lowermost stratosphere, *J. Geophys. Res.*, *112*, D12S04, doi:10.1029/2006JD007664.

## 1. Introduction

[2] Reactive nitrogen species play a central role in the chemistry of the polluted and unpolluted atmosphere. They critically determine levels of ozone, acidity, and atmospheric oxidation potential [*Crutzen*, 1979; *Singh et al.*, 2003a]. When deposited, they act as nutrients in terrestrial and marine ecosystems. The main known constituents of reactive nitrogen in the troposphere are NO, $NO_2$, peroxyacyl nitrates (PANs; $RC(O)OONO_2$), nitric acid ($HNO_3$), peroxynitric acid ($HO_2NO_2$), alkyl and multifunctional nitrates ($RONO_2$), and particulate nitrate ($NO_3^-$). Other less abundant constituents such as HONO, $NO_3$, and $N_2O_5$ play an important role in nighttime chemistry but are quickly decomposed in sunlight [*Brown et al.*, 2006]. Similarly, somewhat long-lived species such as HCN and $CH_3CN$ (lifetime $\approx$ 6 months) are globally abundant products of biomass combustion [*Singh et al.,* 2003b, and references therein]. In most previous studies it was only possible to measure a subset of these reactive nitrogen species and often the data were limited to the LT. The Intercontinental Chemical Transport Experiment-A (INTEX-A) offered a unique opportunity to investigate the partitioning and distribution of reactive nitrogen species

[1]NASA Ames Research Center, Moffett Field, California, USA.
[2]NASA Langley Research Center, Hampton, Virginia, USA.
[3]Department of Chemistry, University of California, Irvine, California, USA.
[4]Department of Chemistry and Department of Earth and Planetary Sciences, University of California, Berkeley, California, USA.
[5]Institute for the Study of Earth Oceans and Space, University of New Hampshire, Durham, New Hampshire, USA.
[6]School of Earth and Atmospheric Sciences, Georgia Institute of Technology, Atlanta, Georgia, USA.
[7]Department of Earth and Planetary Sciences, Harvard University, Cambridge, Massachusetts, USA.
[8]National Center for Atmospheric Research, Boulder, Colorado, USA.
[9]Department of Chemical and Biochemical Engineering, University of Iowa, Iowa City, Iowa, USA.
[10]NOAA Geophysical Fluid Dynamics Laboratory, Princeton, New Jersey, USA.


0148-0227/07/2006JD007664$09.00

from the North American troposphere at a level of detail previously not possible.

[3] INTEX-A was a major field campaign conducted principally over North America and the Atlantic in the summer of 2004 under an international consortium called ICARTT (International Consortium for Atmospheric Research on Transport and Transformation). The ICARTT effort was jointly organized by partners from the United States, Canada, United Kingdom, Germany, and France and its design and implementation was closely coordinated [*Fehsenfeld et al.*, 2006; *Singh et al.*, 2006]. A comprehensive suite of trace gases, aerosols, chemical tracers, and meteorological parameters were measured aboard the NASA DC-8 and its partner aircraft. In this manuscript we mainly use observations from the DC-8 to describe the distribution and partitioning of measured odd nitrogen and its relationship with ozone under polluted and pristine conditions. Observational data are also compared with simulations from multiple models of transport and chemistry to assess our present knowledge of photochemical theory as well as sources and sinks of reactive nitrogen.

## 2. Measurements

[4] The intensive observational phase of INTEX-A was carried out from 1 July to 15 August 2004 over North America. The NASA DC-8 conducted 18 science flights extending from the mid-Pacific to the mid-Atlantic and covered much of the troposphere (0.2–12 km). The most intensive sampling was done over the eastern United States in collaboration with the NOAA P-3 that operated below 7 km altitude. During this period, the UK BAe146 (ceiling 10 km) and the German Falcon (ceiling 13 km) sampled air downwind of North America over the Atlantic Ocean. A map of the geographical extent covered during INTEX-A/ICARTT and a summary of instrumentation and individual flights is provided in the overview papers by *Singh et al.* [2006] and *Fehsenfeld et al.* [2006]. The meteorological description for the region and for each of the missions is described by *Fuelberg et al.* [2007] who also provided detailed 5–10 day back trajectories along DC-8 flight tracks for the entire mission.

[5] The NASA DC-8 aircraft was equipped with several in situ instruments measuring ozone, reactive nitrogen and hydrogen species, aerosol composition and microphysics, and a variety of chemical tracers. Nitrogen containing constituents measured aboard the NASA DC-8 included NO, $NO_2$, $HNO_3$, $HO_2NO_2$, PAN, PPN, alkyl nitrates, aerosol nitrate, HCN, and $CH_3CN$. Observations of $NO_3$ and $N_2O_5$, measured on the NOAA P-3, were also available for analysis [*Brown et al.*, 2006]. The methods used to measure these species have been previously published and are summarized by *Singh et al.* [2006] and *Fehsenfeld et al.* [2006]. Simply stated, ozone was measured by $NO/O_3$ chemiluminescence, PANs by electron-capture gas-chromatography (GC), $HO_2NO_2$ by Chemical Ionization Mass Spectrometry (CIMS), nitric acid by mist chamber/IC analysis, aerosol nitrate by filter collection/IC analysis, hydrocarbons/simple alkyl nitrates by grab sampling and subsequent GC-FID/MS analysis, $NO_2$ by a Laser-Induced-Fluorescence (LIF), NO by chemiluminescence, and nitriles by GC using a Reduction Gas Detector. The sum of all peroxyacyl nitrates ($\sum$PANs) and of alkyl and multifunctional nitrates ($\sum$ANs) were measured using thermal dissociation (TD) and LIF detection of $NO_2$ [*Day et al.*, 2002]. Note we define the sum of the simple alkyl nitrates as $\Sigma RONO_2$ and refer to measurements of this entire class of species as $\Sigma$ANs in this manuscript.

[6] A fast response CIMS instrument on the NOAA P-3 [*Flocke et al.*, 2005] measured PAN and PPN, which were found to be linearly correlated ([PPN] = 0.11 [PAN]; $R^2$ = 0.86). We have used this relationship for estimating PPN from PAN when appropriate. We also note that the NO instrument on the DC-8 had limited sensitivity and was only suitable for measuring mixing ratios >100 ppt. NO calculated from $NO_2$ data (sensitivity $\approx$ 10 ppt) using a steady state box model [*Crawford et al.*, 1999] agreed well with measured values for NO > 100 ppt. To obtain a uniform data set we have defined $NO_x$ as the sum of measured $NO_2$ and calculated NO.

## 3. Data Analysis and Models

[7] Merged data files were created to align species measured with varying time resolutions and these files are used in this study. We have also used a variety of chemical and meteorological filters for purposes of air mass characterization. The principal chemical filter for this study was based on CO mixing ratios. When CO data were unavailable, $C_2H_6$ or $C_2H_2$ observations, which tended to be linearly correlated with CO, were used to fill data gaps. Although INTEX-A data were principally obtained in the troposphere, stratospheric influences were frequently encountered. Two stratospherically influenced data subsets were created. These included a stringent subset ($O_3$ > 200 ppb; CO < 60 ppb; and Z > 7 km) used primarily for defining the composition of the lowermost stratosphere (LMS). A somewhat looser definition ($O_3$ > 120 ppb; $H_2O$ < 100 ppm and Z > 7 km) was employed to remove mixed stratospheric/tropospheric influences from the tropospheric subset. Tropospheric data were further divided into (1) clean background (CO: 60–90 ppb or $C_2H_6$: 250–600 ppt), (2) polluted air masses (CO: 90–240 ppb or $C_2H_6$: 600–3000 ppt), and (3) episodic (CO > 240 ppb or $C_2H_6$ > 3000 ppt). Figures 1a and 1b show the atmospheric distribution of HCN and CO for these subsets. HCN is a unique tracer of biomass combustion [*Singh et al.*, 2003b] while CO is a more generic tracer of all pollution. It is evident from HCN profiles that biomass burning influences were present throughout the troposphere during all periods of pollution. Episodic events contained enhanced signatures of biomass combustion. Furthermore, both HCN and CO profiles provided a reasonable description of what can be expected to be present in the clean background air from historical data in this season [*Holloway et al.*, 2000; *Zhao et al.*, 2002; *Edwards et al.*, 2004]. Multiple tracers were also used to identify specific plumes originating from forest fires, anthropogenic emissions, convection and lightning, and the stratosphere. Data were also segregated geographically to represent Pacific, Atlantic, and continental regions. Total reactive nitrogen ($NO_y$), was defined as follows:

$$NO_y = NO + NO_2 + HNO_3 + PAN + PPN + HO_2NO_2 + \Sigma RONO_2 + NO_3^-$$

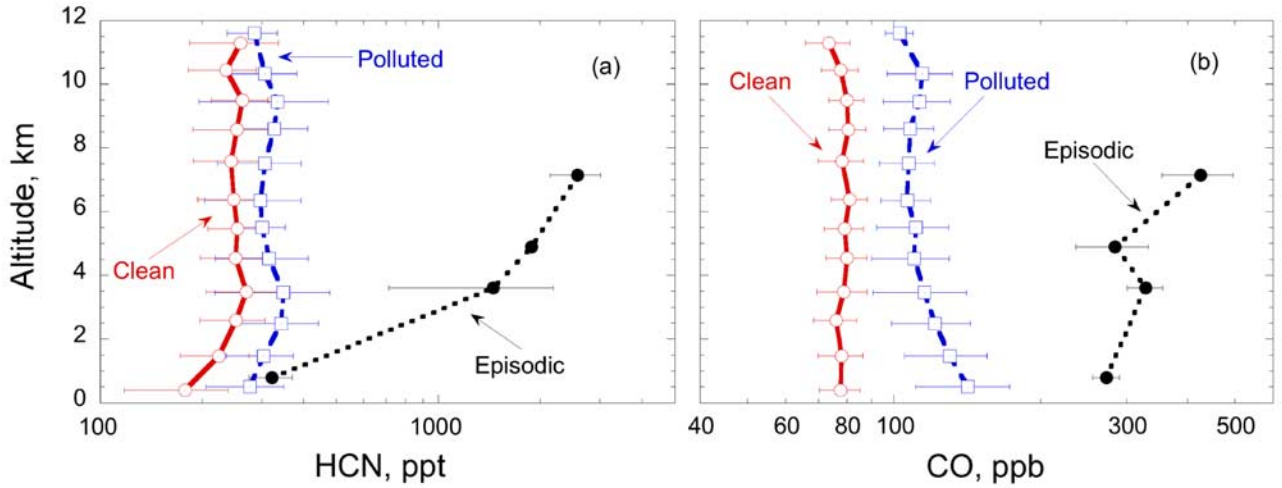


**Figure 1.** Distribution of two selected tracer species ((a) HCN and (b) CO) under "background," "polluted," and "episodic" conditions. See text for more detail.

In several previous studies the extent to which aerosol nitrate was sampled as $NO_y$ has not been accurately identified [*Miyazaki et al.*, 2005]. During INTEX-A, aerosol nitrate was a small fraction of the total $NO_y$ and has been included. $N_2O_5$ and $NO_3$ concentrations, as measured on the NOAA P-3, were extremely low and contributed negligibly to $NO_y$ during daytime and minimally (<0.1% for Z > 1 km) at night [*Brown et al.*, 2006]. The above definition of $NO_y$ also omits the complex organic nitrates observed as ΣANs resulting in some bias due to this omission in the boundary layer.

[8] The data collected during INTEX-A were compared with results from three global and one regional chemical transport models (CTMs). The three global CTMs used in this study included GEOS-CHEM [*Bey et al.*, 2001; *Hudman et al.*, 2007], MOZART [*Horowitz et al.*, 2003; *Pfister et al.*, 2005], and RAQMS [*Pierce et al.*, 2003, 2007]. The global models had a 2° x 2.5° nominal resolution. The regional model STEM had finer resolution and derived its boundary conditions from the MOZART global model [*Tang et al.*, 2004, 2007]. The meteorological and emission fields input into these models were determined independently by each group. The total global $NO_x$ source in these models varied from 40 to 50 Tg N $yr^{-1}$. However, the distribution of these emissions varied according to the model. For example, global lightning source of $NO_x$ (Tg N $yr^{-1}$) in RAQMS, GEOS-CHEM, and MOZART was 3, 5, and 9 respectively, prior to adjustment of the lightning $NO_x$ source to match the profiles observed during INTEX-A. More details on these models and their simulation techniques are

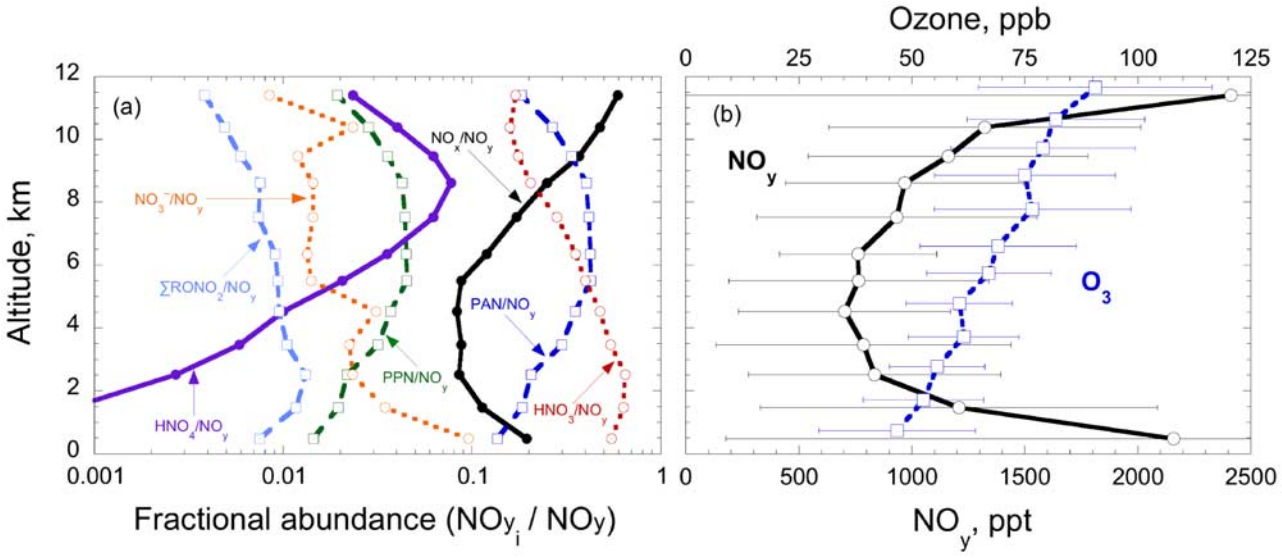


**Figure 2.** (a) Partitioning of reactive nitrogen in the troposphere and (b) the mean vertical structure of $O_3$ and $NO_y$ based on INTEX-A observations.

**Table 1.** Reactive Nitrogen, $O_3$, and CO Mixing Ratios in the North American Troposphere During INTEX-A

| Altitude, km | $O_3$, ppb | CO, ppb | $NO_x$, ppt | $HNO_3$, ppt | PAN, ppt | PPN, ppt | $HO_2NO_2$, ppt | $NO_3^-$, ppt | $NO_y$, ppt | $\sum RONO_2$, ppt | HCN, ppt | $CH_3CN$, ppt |
|---|---|---|---|---|---|---|---|---|---|---|---|---|
| 0–2 | 48.9 ± 16.2 (48.4, 2607)[a] | 132.1 ± 37.2 (127.4, 2079) | 379 ± 823 (148, 1866) | 893 ± 824 (701, 2467) | 301 ± 339 (186, 1666) | 32 ± 36 (20, 1666) | 5 ± 8 (2, 78) | 154 ± 183 (101, 1834) | 1781 ± 1699 (1374, 1283) | 18 ± 13 (15, 1473) | 274 ± 76 (267, 1007) | 136 ± 35 (132, 1007) |
| 2–4 | 58.7 ± 11.8 (58.4, 1332) | 112.7 ± 35.3 (107.6, 1107) | 64 ± 63 (52, 975) | 488 ± 358 (404, 1279) | 214 ± 245 (158, 1021) | 23 ± 26 (17, 1021) | 10 ± 23 (2, 615) | 110 ± 180 (34, 418) | 809 ± 610 (652, 766) | 11 ± 7 (9, 899) | 337 ± 172 (310, 582) | 153 ± 80 (138, 587) |
| 4–6 | 63.3 ± 13.1 (62.6, 1268) | 103.3 ± 26.7 (99.6, 1027) | 54 ± 39 (47, 976) | 317 ± 234 (269, 1216) | 275 ± 228 (217, 981) | 29 ± 24 (23, 981) | 15 ± 31 (8, 1094) | 90 ± 202 (10, 511) | 733 ± 523 (613, 737) | 9 ± 4 (8, 828) | 296 ± 121 (285, 563) | 144 ± 69 (136, 570) |
| 6–8 | 72.4 ± 19.7 (71.3, 1492) | 104.7 ± 51.8 (96.9, 1241) | 113 ± 85 (92, 1154) | 252 ± 185 (210, 1415) | 354 ± 253 (298, 1106) | 38 ± 27 (32, 1106) | 41 ± 34 (31, 1353) | 58 ± 202 (13, 786) | 849 ± 511 (755, 856) | 9 ± 5 (8, 907) | 308 ± 258 (273, 630) | 148 ± 97 (137, 667) |
| 8–10 | 76.6 ± 20.2 (74.3, 1523) | 102.3 ± 20.9 (101.3, 1175) | 323 ± 288 (240, 1256) | 202 ± 186 (146, 1497) | 371 ± 217 (339, 1138) | 39 ± 23 (36, 1138) | 73 ± 40 (66, 1406) | 27 ± 45 (11, 909) | 1040 ± 570 (931, 923) | 10 ± 6 (9, 954) | 315 ± 138 (297, 595) | 138 ± 40 (133, 720) |
| 10–12 | 82.7 ± 20.5 (82.2, 942) | 96.5 ± 22.8 (93.7, 687) | 776 ± 900 (552, 700) | 205 ± 153 (159, 901) | 338 ± 208 (295, 650) | 36 ± 22 (31, 650) | 53 ± 30 (49, 868) | 34 ± 60 (21, 818) | 1430 ± 1052 (1197, 465) | 8 ± 6 (7, 586) | 274 ± 73 (284, 404) | 141 ± 20 (141, 406) |
| 0–12 | 64.2 ± 20.9 (62.9, 9164) | 112.3 ± 37.8 (106.2, 7316) | 275 ± 572 (106, 6927) | 462 ± 558 (285, 8775) | 308 ± 269 (246, 6562) | 33 ± 28 (26, 6562) | 42 ± 41 (29, 5414) | 90 ± 167 (28, 5276) | 1152 ± 1099 (829, 5030) | 12 ± 9 (9, 5647) | 299 ± 153 (285, 3781) | 142 ± 63 (136, 3967) |

[a]Mean ± sigma (median, number of points).



**Table 2.** Alkyl Nitrate ($C_1$-$C_5$) Mixing Ratios in the North American Troposphere During INTEX-A

| Altitude, km | $CH_3ONO_2$, ppt | $C_2H_5ONO_2$, ppt | i-$C_3H_8ONO_2$, ppt | n-$C_3H_8ONO_2$, ppt | 2-$C_4H_{10}ONO_2$, ppt | 3-$C_5H_{12}ONO_2$, ppt | 2-$C_5H_{12}ONO_2$, ppt | $\sum RONO_2$, ppt | $\sum$ANs,[a] ppt |
|---|---|---|---|---|---|---|---|---|---|
| 0–2 | 2.3 ± 0.7 (2.1, 1467) [b] | 2.3 ± 1.1 (2.0, 1467) | 5.4 ± 4.0 (4.4, 1467) | 0.7 ± 0.5 (0.6, 1467) | 4.6 ± 4.5 (3.5, 1467) | 1.4 ± 1.4 (1.1, 1469) | 1.8 ± 2.0 (1.3, 1473) | 18 ± 13 (15, 1473) | 191 ± 204 (147, 1713) |
| 2–7 | 1.9 ± 0.4 (1.9, 2198) | 1.5 ± 0.5 (1.5, 2198) | 2.9 ± 1.7 (2.6, 2198) | 0.3 ± 0.2 (0.3, 2198) | 2.1 ± 2.0 (1.6, 2198) | 0.5 ± 0.6 (0.3, 2214) | 0.5 ± 0.7 (0.3, 2219) | 10 ± 6 (9, 2219) | |
| 7–12 | 2.1 ± 0.5 (2.1, 1890) | 1.7 ± 0.7 (1.6, 1890) | 3.7 ± 3.0 (2.9, 1890) | 0.3 ± 0.2 (0.2, 1900) | 1.5 ± 2.1 (0.7, 1894) | 0.2 ± 0.5 (0.1, 1936) | 0.1 ± 0.3 (0.0, 1950) | 10 ± 6 (8, 1950) | |

[a]Sum of alkyl nitrates ($\sum$ANs) was measured in the lower troposphere (Z < 4 km) by thermally dissociating these to $NO_2$ (see text).
[b]Mean ± sigma (median, number of points).

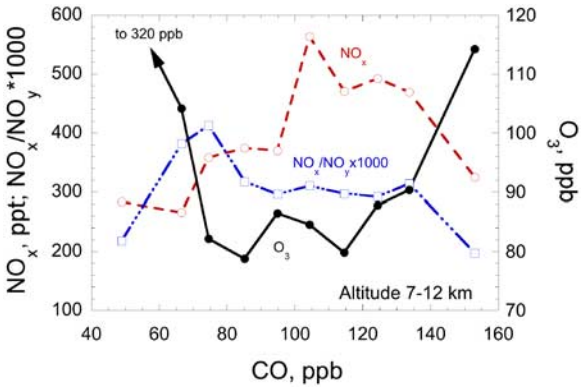


**Figure 3.** Mean mixing ratios of $NO_x$ and $O_3$ as a function of CO. The data are binned for 7–12 km altitude and show the transition from the upper troposphere to lowermost stratosphere. Larger $NO_x/NO_y$ ratios indicate more recent $NO_x$ injections.

being published separately [*Hudman et al.*, 2007; *Pierce et al.*, 2007; *Tang et al.*, 2007].

## 4. Results and Discussion

### 4.1. Partitioning and Atmospheric Behavior of Reactive Nitrogen

[9] Figures 2a and 2b show the partitioning of reactive nitrogen in the troposphere and the mean vertical structure of $O_3$ and $NO_y$ based on data collected in INTEX-A. Table 1 provides additional statistical information on the vertical structure of selected reactive nitrogen and tracer species. Table 2 shows the breakdown of individual $C_1$–$C_5$ alkyl nitrates, whose sum is presented in Figure 2a and Table 1, in altitude bins representing lower troposphere (LT; 0–2 km), middle troposphere (MT; 2–7 km) and upper troposphere (UT; 7–12 km). The measured sum of alkyl nitrates ($\sum$ANs) in the boundary layer was approximately 10 times larger than the sum of individually measured straight chain alkyl nitrates (Table 2), indicating the dominance of more complex organic nitrates. Calculations of the alkyl nitrate production rate following the methods outlined by *Rosen et al.* [2004] and *Cleary et al.* [2005] and using the observed VOC, indicate that isoprene oxidation is by far the largest single source of $RONO_2$ in the boundary layer. The sum of isoprene nitrate and other alkyl and multifunctional nitrates contribute about 10% to the mean $NO_y$ in the continental boundary layer. *Horowitz et al.* [2007] have used these observations along with a CTM to constrain the chemistry of isoprene nitrate production and loss and the isoprene nitrate deposition rate. They find that relatively slow production rates, fast loss rates, and fast deposition velocities are required to match the data. All of these combine to reduce the concentration of isoprene nitrates relative to options employed in other models.

[10] It is evident from Figure 2a that although reactive nitrogen is principally emitted as NO, throughout much of the troposphere it largely exists in its secondary reservoir forms. The total column of $NO_x$ in the troposphere constituted only about 15% of available $NO_y$. PAN and $HNO_3$ together contained around 65% of $NO_y$, with PAN dominating in the UT and $HNO_3$ in the LT. A moderate fraction (≈5%) of reactive nitrogen in the UT was also due to $HO_2NO_2$, which was directly measured for the first time in this mission [*Huey et al.*, 2007]. Gaseous and aerosol nitrates comprised a very small fraction (<5%) of the tropospheric $NO_y$ reservoir. $NO_x$ was the dominant reactive nitrogen species at altitudes above 9 km (Figure 2a). As stated earlier, higher organic nitrates (e.g., isoprene nitrate) may contribute up to 10% to $NO_y$ in the continental boundary layer. Unlike $O_3$, which increased monotonically with altitude (Figure 2b), $NO_y$ showed a C-shaped profile with high concentrations near the surface and in the UT.

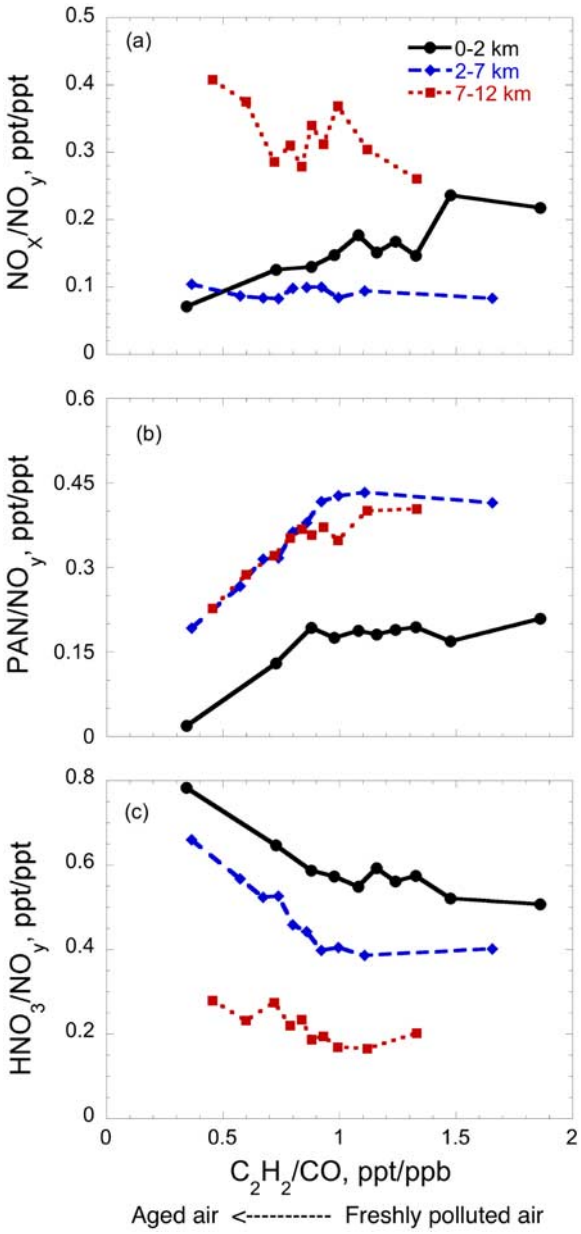


**Figure 4.** Reactive nitrogen as a function of air mass age in the lower (0–2 km), middle (2–7 km) and upper (7–12 km) troposphere (latitude: 30–50°N, longitude: 260–320°E). Air mass age is defined with reference to time from emission ("chemical clock"). All data were divided into 10 age bins. Each point shown above represents an average of 60–120 observed data points.

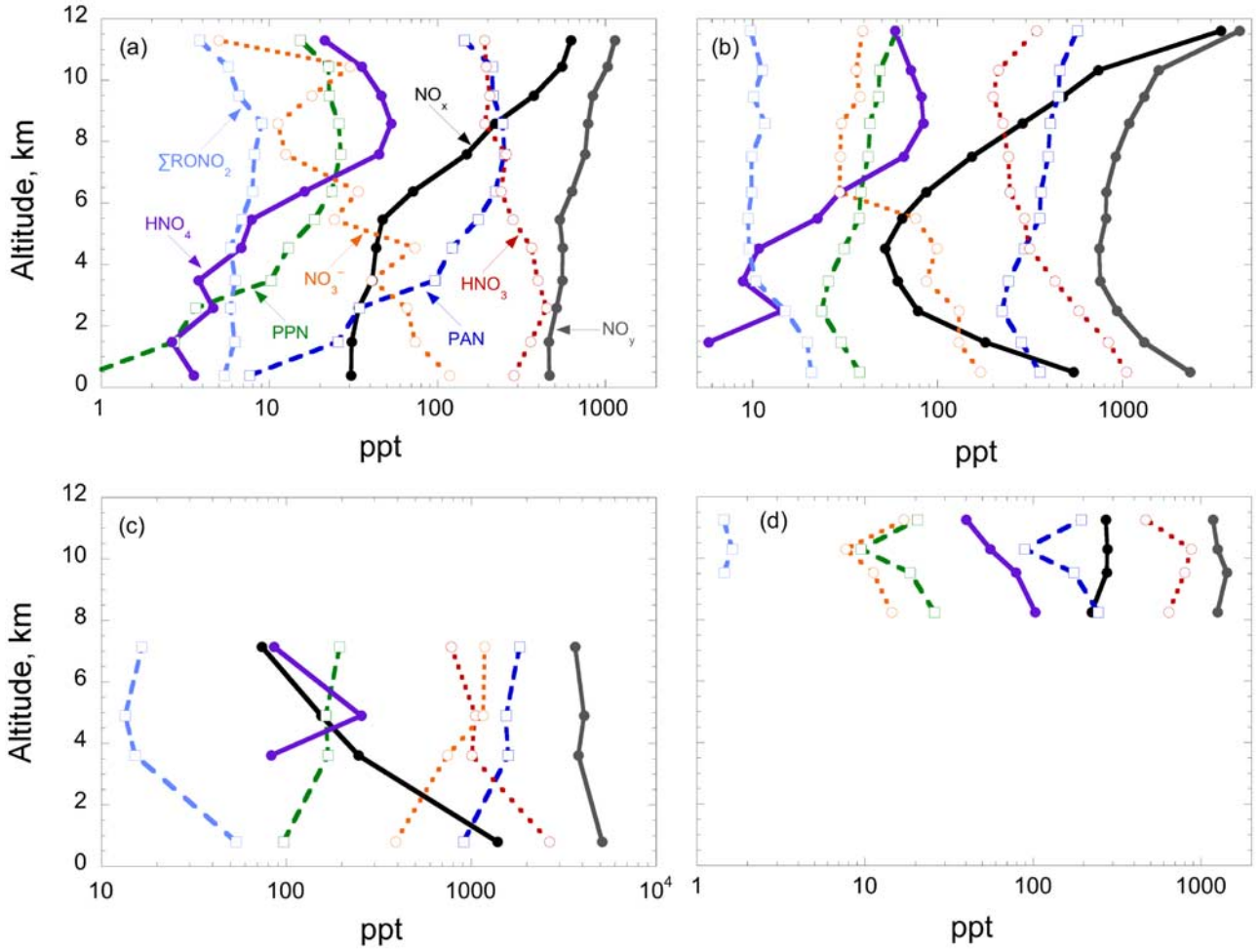


**Figure 5.** Reactive nitrogen species in the troposphere and lowermost stratosphere. (a) "Background/clean," (b) "polluted," (c) "episodic," and (d) "lowermost stratospheric." See text for more detail.

[11] Figure 3 shows a plot of $NO_x$, $NO_x/NO_y$, and $O_3$ as a function of CO for the 7–12 km altitude bin. CO is chosen as a convenient tracer that can be used to indicate stratospheric influences (low CO) as well as pollution (high CO). The UT mean $NO_x$ mixing ratios of 300–500 ppt observed during INTEX-A were similar to those previously reported by *Brunner et al.* [2001] from eastern North America and can be considered fairly typical of the summer period. Mean $NO_x/NO_y$ ratios (0.2–0.4) exceeded by a factor of two or more those found in the polluted surface layer and values reported from the midlatitude UT downwind of Asia [*Singh et al.*, 1996; *Kondo et al.*, 1997] and North America [*Jaegle et al.*, 1998; *Singh et al.*, 1999; *Koike et al.*, 2000]. These high $NO_x/NO_y$ ratios provide a direct indication of the relative freshness of UT $NO_x$ sources. $NO_x$ levels in the LMS (mean $O_3$-320 ppb) were generally elevated but significantly lower than in the UT. The influence of pollution on UT $O_3$ was also evident and was generally consistent with the calculated net $O_3$ production rate of about 5 ppb $day^{-1}$ at these $NO_x$ levels. Aged and polluted air masses indicated by high CO and lower $NO_x/NO_y$, where photochemistry has occurred over a longer time period, were seen to be associated with large $O_3$ concentrations.

[12] In many previous studies, the $C_2H_2$/CO ratio has been used as a "chemical clock" to provide a qualitative measure of air mass age since emission. Figure 4 shows a plot of the fractional reactive nitrogen abundance of key species as a function of this age. Because of the relatively short lifetime of $NO_x$ compared to $NO_y$, $NO_x/NO_y$ is expected to decrease with increasing air mass age. This was clearly found to be the case in the LT (Figure 4a) where the lifetime of $NO_x$ is short (<0.5 days) and $NO_x/NO_y$ decreased by a factor of 3 with age. In the MT (2–7 km), the $NO_x/NO_y$ ratio was both low (≈0.1) and nearly independent of age. We believe that this is indicative of the existence of a steady state between the $NO_y$ reservoir species and $NO_x$ {PAN ⟷ $NO_2$ + PA; $HNO_3$ + h$\nu$ ⟷ $NO_2$ + OH; $HNO_3$ + OH → $NO_2$ + O + $H_2O$}. Model calculations by *Jaegle et al.* [1998] show that a $NO_x/NO_y$ ratio in steady state should be between 0.05 and 0.1 in the troposphere. These low $NO_x/NO_y$ ratios were also seen in extremely aged air masses in the LT.

[13] The UT region (7–12 km) behaved completely differently with high $NO_x/NO_y$ ratios that also increased as a function of age. This is only possible if fresh injections of $NO_x$ are being made in the UT. Benzene ($C_6H_6$) is a

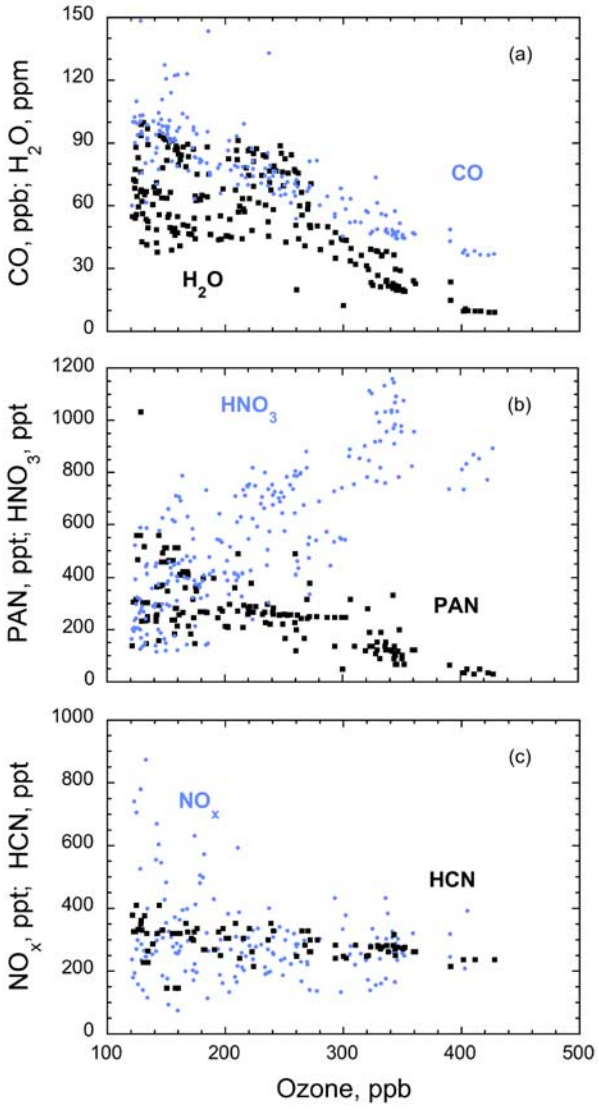


**Figure 6.** Mixing ratios of key tracer and reactive nitrogen species in the lowermost stratosphere sampled in INTEX-A.

hydrocarbon of surface origin with about a 7-day lifetime, slightly longer than $NO_x$. $NO_x/C_6H_6$ ratios of about 60 during convective conditions in the UT were significantly higher than the ratios of about 10 observed in the boundary layer even under polluted conditions. This suggests that lofting of surface $NO_x$ by convection could not have contributed more than 20% to the UT $NO_x$. *Bertram et al.* [2007] analyze the deviation from steady state to show the mean fraction of the UT that is lofted boundary layer air after convection is 17%. Since the mean $NO_x$ in the PBL is on average about half that seen in the UT, this result implies that about 9% of UT $NO_x$ is due to lofted PBL air. Unlike the MT, a steady state with $NO_y$ reservoir species was not achieved in the UT.

[14] During the summer of 2004, wide spread lightning throughout central and eastern North America was observed (M. H. Porter et al., unpublished manuscript, 2006). A gridded (11 km x 11 km) inventory of lightning flashes (cloud-to-ground) over the United States during the entire INTEX-A period showed 100–250 flashes nearly everywhere east of 110°W with large regions of 500–1600 flash counts. Comparison with previous 6 years suggests that these lighting flash frequencies were slightly above average (≈10%) but fairly typical of the summer season. However, lightning sources over North America during INTEX-A required to reproduce the observed UT $NO_x$ were 4–8 times what was assumed in the models (0.4 TgN $y^{-1}$) [*Martin et al.*, 2006; *Hudman et al.*, 2007; *Cooper et al.*, 2006]. Aircraft emissions add some 0.5 TgN $y^{-1}$ to the UT globally [*Brasseur et al.*, 1998]. We estimate that over North America these emissions (≈0.1 TgN $y^{-1}$) contribute less than 50 ppt to UT $NO_x$ and made only a small contribution in comparison with lightning effects. As is seen from Figure 3, the lower stratosphere contained much less $NO_x$ than the UT and hence was a minimal contributor. Observations performed over North America in the spring during the SUCCESS campaign showed substantially lower $NO_x/NO_y$ ratios in the UT (≈0.15) compared to INTEX-A (≈0.3). This is consistent with the seasonal cycle in $NO_x$ reported by *Brunner et al.* [2001] and with the seasonal cycle in lightning.

[15] Unlike $NO_x$, the response of PAN and $HNO_3$ to aging was similar at all altitudes (Figure 4). The relative fraction of PAN declined with air mass age, while that of $HNO_3$ increased. The net increase in $HNO_3$ with age closely approximated the decrease in PAN. This is consistent with the notion that the PAN reservoir ultimately exerts substantial control on $NO_x$ and subsequently $HNO_3$. A separate analysis of PAN chemistry shows PAN is nearly constant once injected into the upper troposphere indicating that most of the aging we observe has occurred in the PBL or MT prior to convection [*Bertram et al.*, 2007].

### 4.2. Distribution of Reactive Nitrogen

#### 4.2.1. Reactive Gaseous Nitrogen

[16] Figures 5a–5d show the abundance of reactive nitrogen species under "characteristic" conditions in the troposphere and the LMS. Under "clean" or "near background" conditions (Figure 5a), PAN and $NO_x$ were extremely low in the LT where $HNO_3$ dominated. PAN gradually increased with altitude and in the UT was nearly as abundant as $HNO_3$. $NO_x$ mixing ratios increased rapidly above 6 km and became dominant above 8 km. $HO_2NO_2$ was present in sizable mixing ratios in the UT peaking at about 9 km. $HO_2NO_2$, which is highly unstable thermally and easily decomposed at temperatures below 6 km ($\tau$ < 1 hours), was present in sizable mixing ratios in the UT peaking at about 8 km. Above 8 km, its loss is slower ($\tau$ = 6–8 hours) mostly determined by reaction with OH and photolysis. The maximum observed at about 8 km coincided with a region of minimum loss. At even higher altitudes the loss rate is nearly constant but production rates are smaller because of reduced $HO_2$ mixing ratios (X. Ren et al., HOx observation and model comparison during INTEX-NA 2004, unpublished manuscript, 2007, hereinafter referred to as Ren et al., unpublished manuscript, 2007) and air density ($HO_2 + NO_2 + M \rightarrow HO_2NO_2$). In the polluted subset (Figure 5b) nearly all reactive nitrogen concentrations were elevated compared to the background (Figure 5a) and a C-shaped profile with large values in the UT and LT was present for both $NO_x$ and $NO_y$. A dramatic change

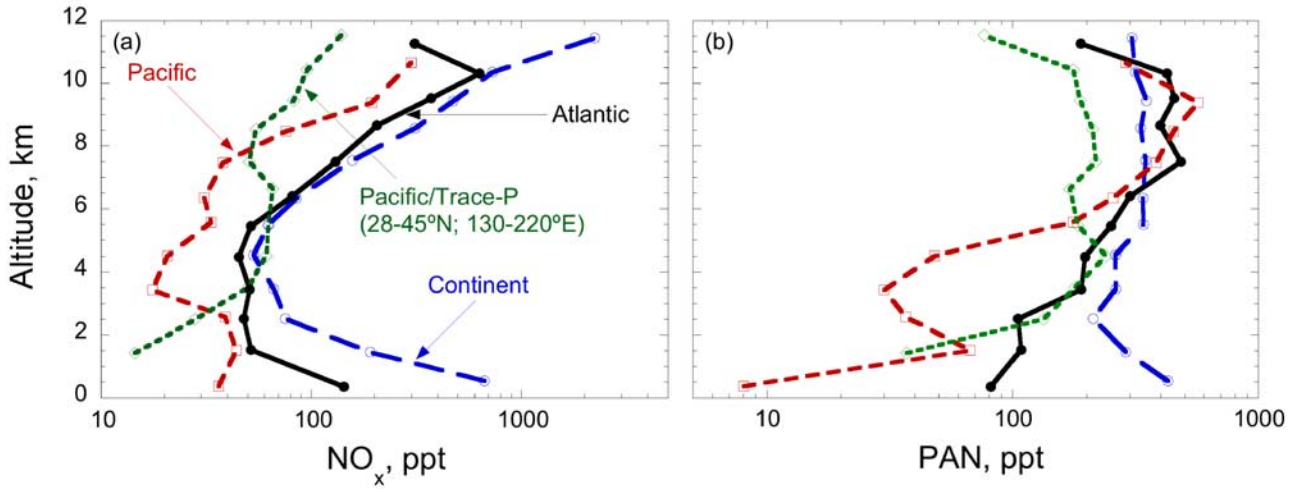


**Figure 7.** (a) $NO_x$ and (b) PAN over the Pacific, continental North America, and the western Atlantic.

could be seen in PAN, which was now significantly more abundant than $HNO_3$ at all altitudes above 4 km. $HO_2NO_2$ still peaked at 9 km but was nearly twice as abundant as under clean conditions largely because of the higher $NO_x$ (as well as $HO_x$) available under these conditions. Under all conditions, the $NO_x$ levels in the UT were larger than their surface values and could not be attributed to surface pollution alone. Under episodic conditions (Figure 5c), involving extreme levels of pollution, $NO_y$ was extremely high (4–6 ppb) and PAN continued to dominate over $HNO_3$ at even lower levels. $HO_2NO_2$ levels of 100–200 ppt, comparable to $NO_x$, were seen within these plumes at moderately low altitudes. Aerosol nitrate was present at concentrations much larger than $NO_x$ in these air masses. The LMS composition was dramatically different where $HNO_3$ and $NO_x$ were the dominant species and PAN was rather low (Figure 5d).

[17] Figures 6a–6c show the transition from the troposphere to the LMS ($O_3$<440 ppb) for a select group of species. The $NO_x$ mixing ratios of 200–300 ppt in the LMS

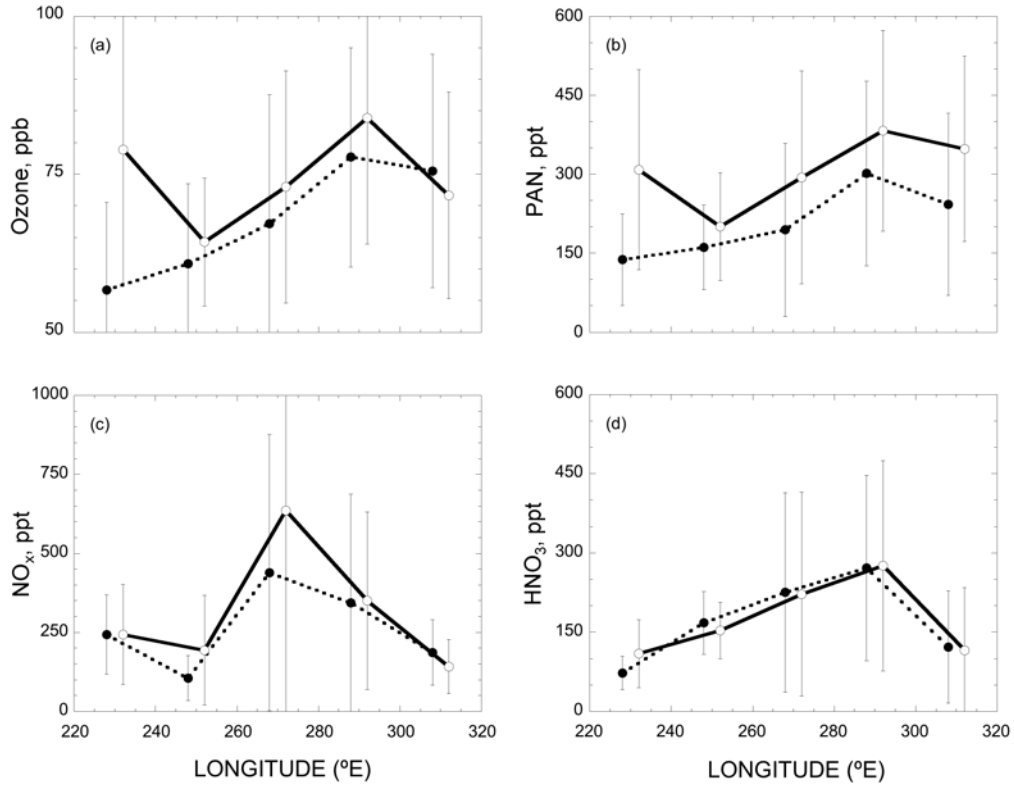


**Figure 8.** Ozone and reactive nitrogen in the North American upper troposphere (7–12 km; 30–45°N) under "all observed" (solid) and "clean" (dashed) conditions.

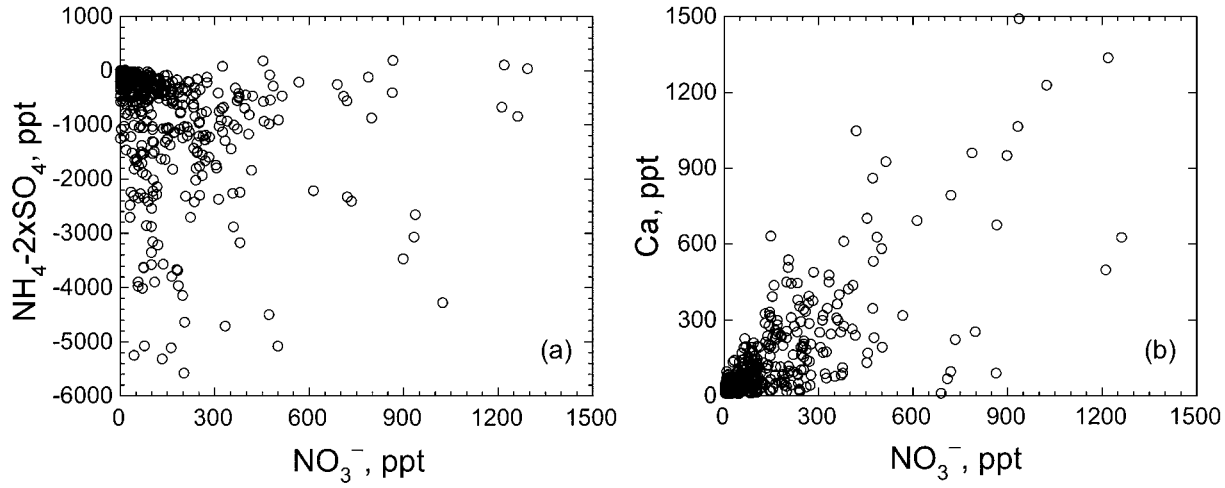


**Figure 9.** Bulk aerosol nitrate relationship with (a) excess sulfate and (b) calcium ion. All aerosol samples are <5 $\mu$m in size.

where steady state with $NO_y$ is likely achieved should be compared with 600–3000 ppt in the UT where convection and lightning are driving the chemistry away from steady state and result in high $NO_x$ (Figures 5a and 5b). Similarly $NO_x/NO_y$ ratio of 0.2 in the LMS can be compared with 0.6 at 12 km. Since $NO_x$ levels in the troposphere continued to rise to the DC-8 ceiling altitude of 12 km, it is likely that a $NO_x$ maximum above this altitude was present with levels subsequently decreasing toward the tropopause. Such high $NO_x$ maxima coincident with lightning conditions have been observed at subtropical latitudes and over Europe [*Huntrieser et al.*, 2002; *Ridley et al.*, 2004]. In the LMS,

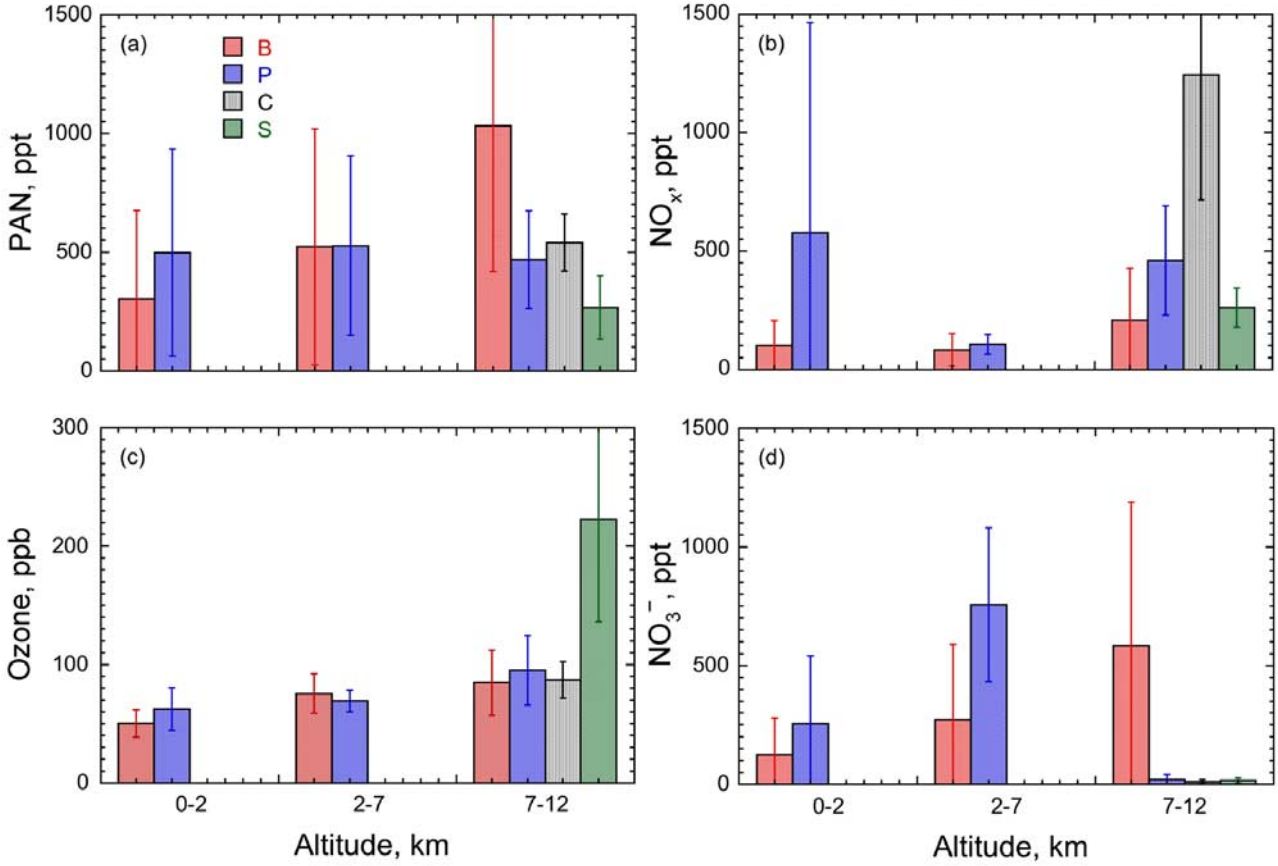


**Figure 10.** Distribution of selected chemicals in plumes influenced by biomass burning (B), anthropogenic pollution (P), lightning/convection (C), and stratosphere (S). Altitude bins are selected to represent the lower, middle, and upper troposphere.

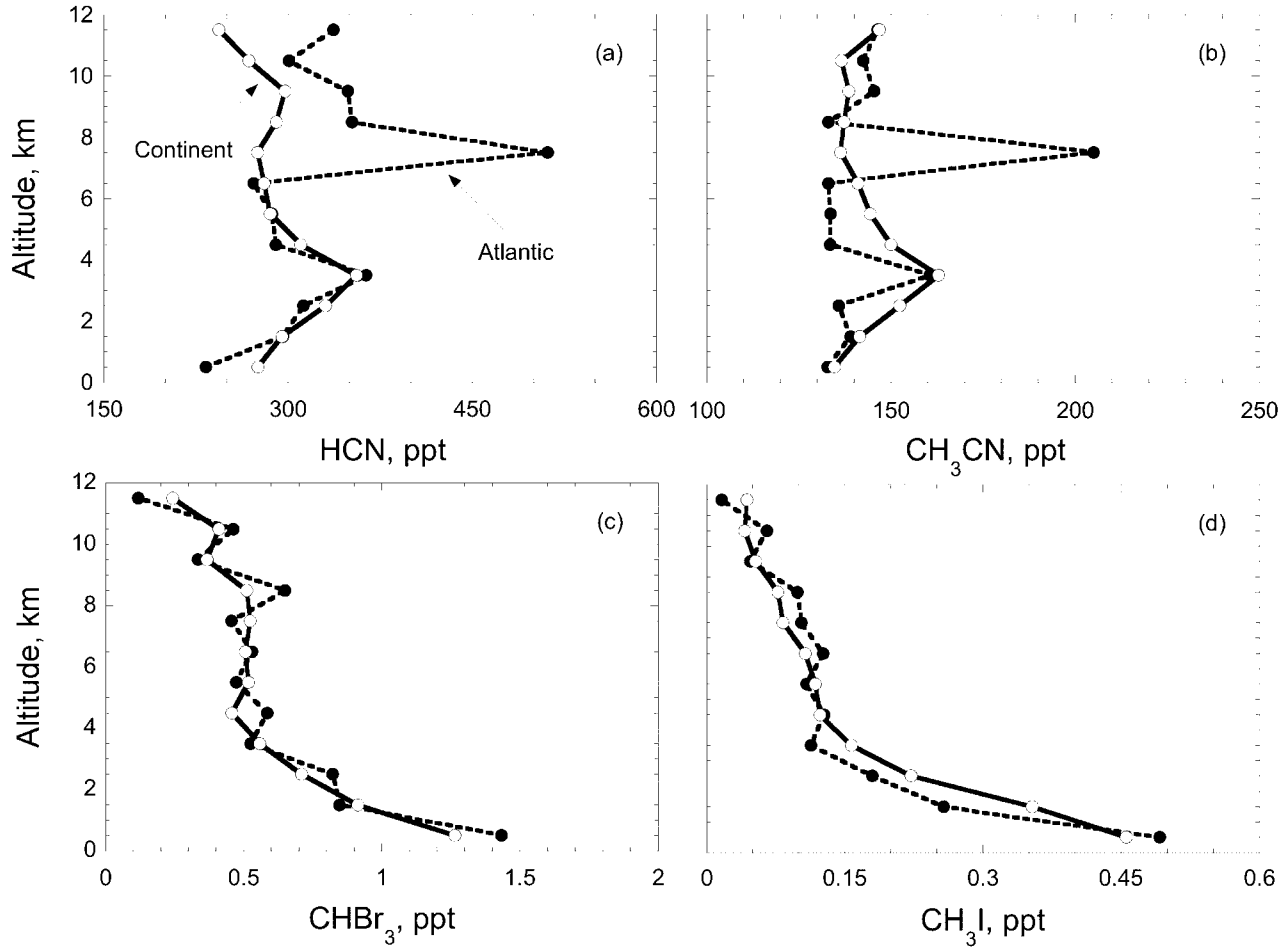


**Figure 11.** Vertical distribution of nitriles and oceanic sourced tracers.

$NO_x$ and HCN levels remained relatively unchanged while PAN, CO, and $H_2O$ declined and $HNO_3$ increased. This behavior was similar to what has been previously reported from other locations and seasons [*Singh et al.*, 1997] and the $NO_x/HNO_3$ ratio is consistent with description of factors affecting $HNO_3/NO_x$ ratios in the lower stratosphere as described by *Perkins et al.* [2001] and *Cohen and Murphy* [2003].

[18] Figures 7a and 7b show the mean vertical structure of $NO_x$ and PAN from west to east over North America. Since only one flight over the Pacific was conducted during INTEX-A, it is likely biased because of the encounter of Asian pollution in the UT. Therefore we have also included the $NO_x$ and PAN distribution over the Pacific observed during Trace-P in the spring 2001. $NO_x$ levels in the UT increase from west to east. Signatures of continental pollution were similarly seen in the LT for PAN although less so in the UT in part because of the relatively long lifetime of PAN in this region. Figure 8 shows the longitudinal variation in the UT abundance of $O_3$ and select reactive nitrogen species both under "all observed" and "clean" conditions. Mean $O_3$ mixing ratios in the UT were enhanced by 10–15 ppb from west to east even under clean conditions with an additional increase of about 5 ppb due to pollution (Figure 8a). This west to increase in UT $O_3$ was also observed from the ozonesonde data analyzed by *Cooper et al.* [2006] and is largely attributable to lightning emissions of $NO_x$. A much larger increase was seen in PAN, an excellent indicator of pollution and photochemical influences (Figure 8b). Lightning and the associated convection had a considerable impact on $NO_x$ over the central US (Figure 8c). The corresponding increase in $HNO_3$ occurs further East and downwind of the convective source (Figure 8d). In short the North American UT appears to be greatly influenced by lightning and pollution resulting in substantial enhancements in ozone, PAN, and other tracers.

#### 4.2.2. Aerosol Nitrogen

[19] Bulk aerosol (<5 $\mu$m size) were filter collected on the DC-8 and their inorganic ion composition determined by methods described by *McNaughton et al.* [2007]. As shown in Table 1, aerosol nitrate ($NO_3^-$) was present in moderately low concentrations (<10% of $NO_y$) mostly in the LT. Aerosol nitrate can be typically formed via reaction of $NH_3$ and nitric acid ($NH_3 + HNO_3 \leftrightarrow NH_4NO_3$). Bulk aerosol nitrate was found to be moderately correlated with $NH_4^+$ ($R^2 = 0.42$) suggesting a chemical form such as $NH_4NO_3$. An examination of the $NH_4^+$ and $SO_4^-$ ion balance (Figure 9a) clearly indicated that throughout this experiment excess sulfate was nearly always present suggesting insufficient ammonia for acid neutralization. This was unlike the

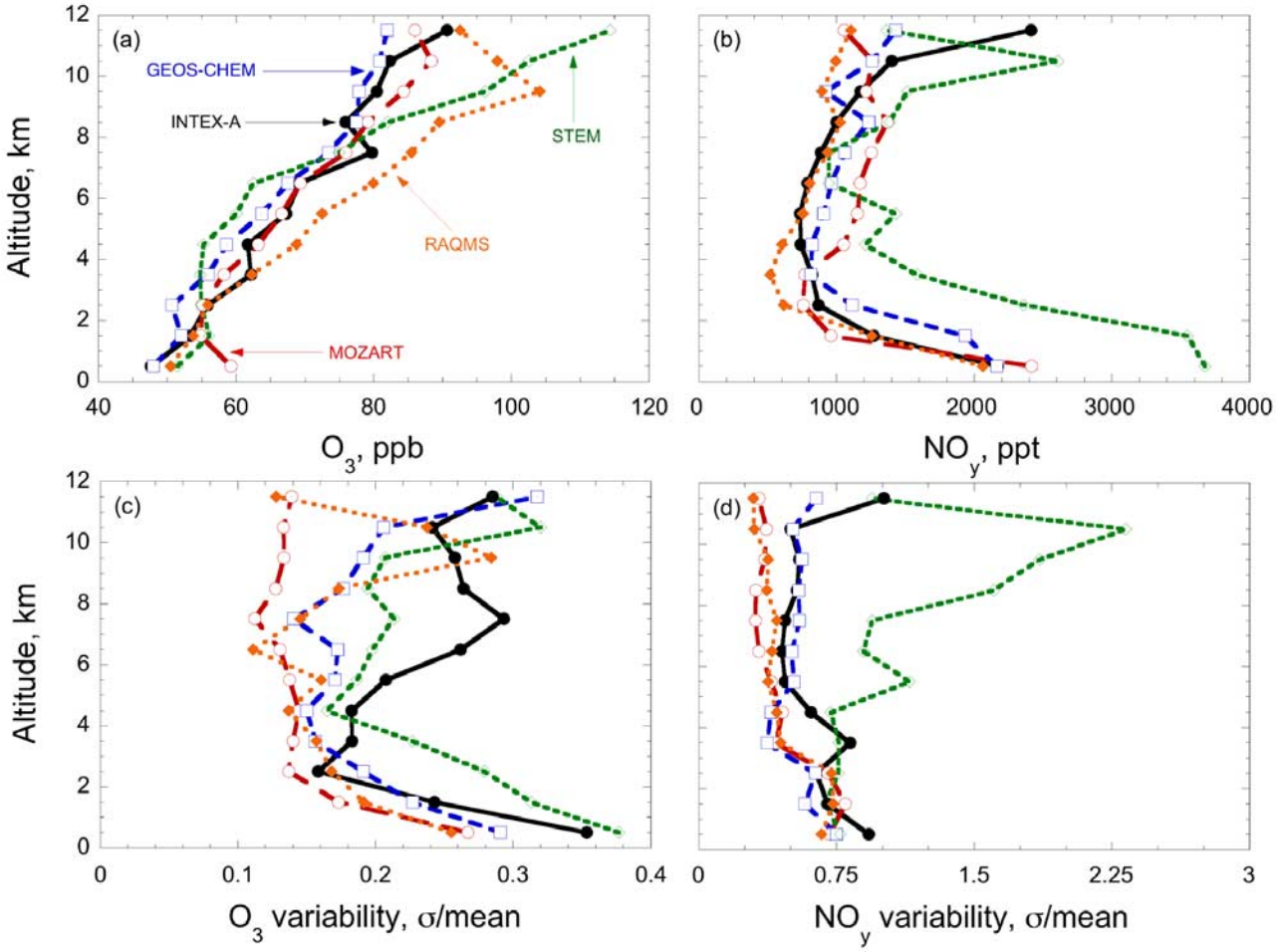


**Figure 12.** Observed and simulated mixing ratios and variability of $O_3$ and $NO_y$ over eastern North America (30–50°N; 260–320°E). (a and b) Mean mixing ratios and (c and d) relative variability.

situation in the Asian pollution outflow where excess ammonium was nearly always present and all $SO_4^-$ had been neutralized [*Miyazaki et al.*, 2005]. Ammonia is preferentially converted to ammonium sulfate as long as $SO_4^-$ is present [*Seinfeld and Pandis*, 1998], and indeed $SO_4^-$ and $NH_4^+$ were highly correlated ($R^2$ = 0.85). We conclude that $NH_4NO_3$ was not the dominant form of the aerosol nitrate observed over North America. Figure 9b further shows that $NO_3^-$ was well correlated with soil elements like calcium. As has been previously noted [*Wolff*, 1984; *Krueger et al.*, 2004], it appears that the source of this aerosol nitrate is $HNO_3$ residing on and reacting with soil and crustal particles that are typically of large size (e.g., $2HNO_3$ (g) + $CaCO_3$ (s) → $Ca(NO_3)_2$ (s)+ $H_2O$ + $CO_2$). This is further supported by the presence of extremely small measured concentrations of submicron $NO_3^-$, which were independently measured in the LT. Unlike $NH_4NO_3$, nonvolatile aerosol nitrate salts represents a nearly permanent sink for reactive nitrogen with virtually no chance of return to the gas phase while in the atmosphere before deposition to the land or ocean.

#### 4.2.3. Plumes

[20] Plumes sampled during INTEX-A were segregated into categories representing influences from biomass burning (BB), anthropogenic pollution (AP), lightning/convection (LC), and the stratosphere (ST). For example, HCN and $CH_3CN$ were highly elevated in BB plumes while high $O_3$ and low CO and $H_2O$ mixing ratios were characteristic of stratospheric influences. Figure 10 shows the distribution of selected species in these plumes as a function of altitude bins representing LT (0–2 km), MT (2–7 km), and UT (7–12 km). Foremost is the appearance of sizable PAN and relatively low $NO_x$ and $O_3$ concentrations in BB plumes (Figures 10a–10c). *Law et al.* [2005] explored the development of some of these plumes over the Atlantic and concluded that net $O_3$ production does eventually occur but is greatly slowed because of the control exerted by PAN on the $NO_x$ reservoir. Another distinct feature was the large $NO_x$ mixing ratios observed in plumes influenced by lightning and convection, which may have frequently coexisted (Figure 10b). Despite the large $NO_x$ values encountered in these LC plumes, $O_3$ was not significantly elevated (Figure 10c). Using the ratio of $NO_x/HNO_3$ as an indicator, *Bertram et al.* [2007] show that $O_3$ is reduced in fresh convection because $O_3$ mixing ratios are lower in the PBL than in the UT. Ozone is then chemically replenished in the convectively lofted air mass on a timescale of 2–3 days. Both $HNO_3$ and aerosol nitrate were significantly elevated

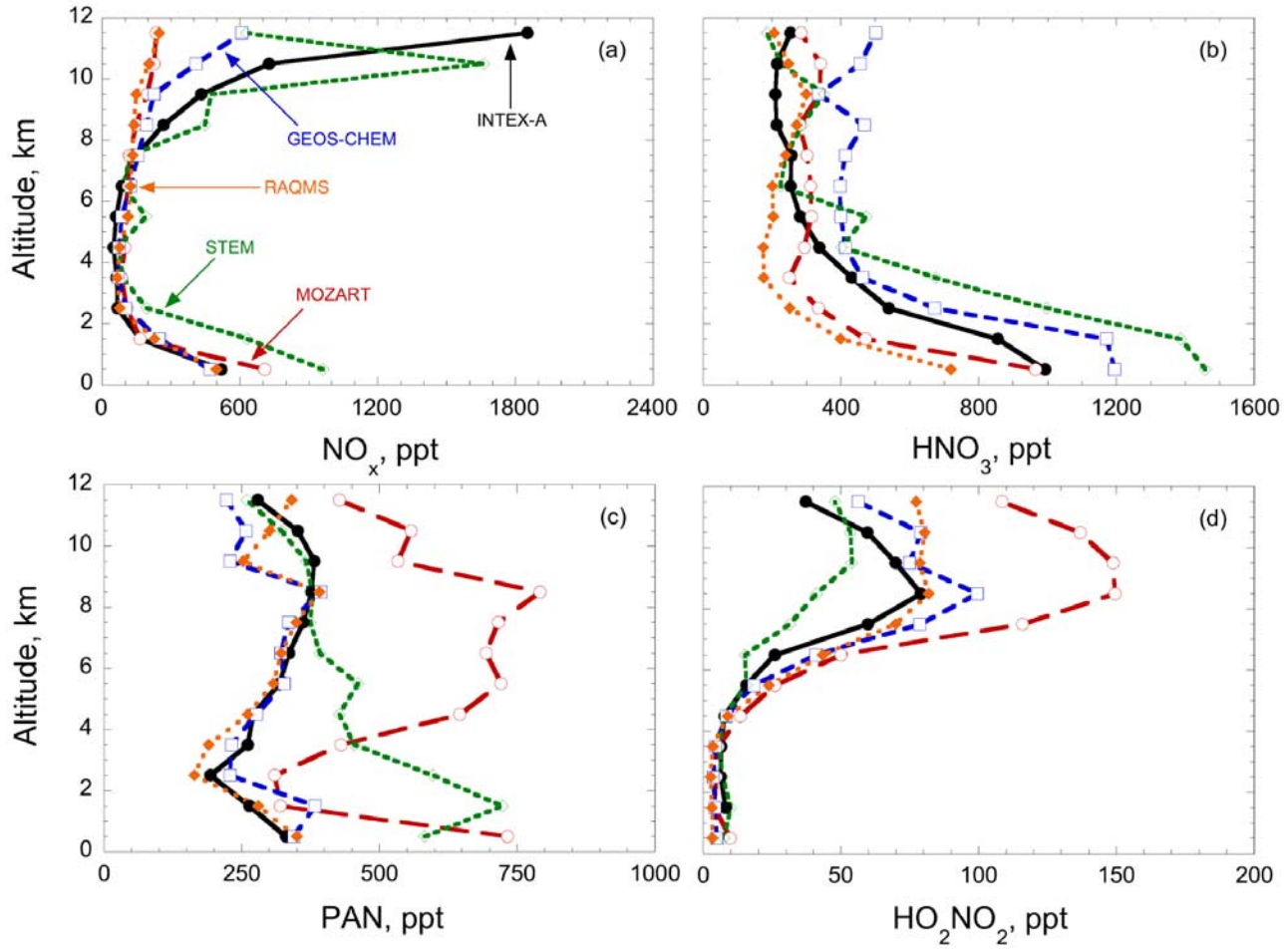


**Figure 13.** Observed and simulated mixing ratios of selected reactive nitrogen species over eastern North America (30–50°N; 260–320°E).

in plumes influenced by anthropogenic and BB pollution (Figure 10d).

#### 4.2.4. Nitrogen Tracers of Biomass Combustion

[21] HCN and $CH_3CN$ are both excellent tracers of biomass combustion and were linearly correlated ($R^2$ = 0.76) in this data set. Figure 11 shows the vertical structure of HCN and $CH_3CN$ over the Atlantic and continental North America. There is an indication of both an oceanic and soil sink for these species. Although an oceanic sink has been recognized, a soil sink is not known and has not been studied [*Singh et al.*, 2003b]. Figure 11 also shows similar profiles for $CHBr_3$ and $CH_3I$, which are both known to have dominant oceanic sources. It is clear from Figure 11 that oceanic influences were widespread in the continental boundary layer. To further explore the potential of soils to act as a sink for nitriles, we used trajectory analysis to compare abundances in air masses that had remained in the boundary layer over land or water for at least 5 days. Overland air masses had mixing ratios of 260 (±20) ppt and 135 (±14) ppt for HCN and $CH_3CN$ while overwater air masses had corresponding mixing ratios of 149 (±33) ppt and 109 (±18) ppt. In short, air masses in long contact with surface water were far more depleted than those in contact with land surfaces. Despite the appearance of a sink, we conclude that HCN and $CH_3CN$ soil sinks were negligible or extremely small. This could be due to low contact time between these molecules and soil bacteria allowing rapid rerelease of deposited nitriles. The column of HCN deduced from these measurements is in good agreement with that reported by *Zhao et al.* [2002] from ground-based spectroscopic measurements over Japan.

### 4.3. Model Simulations

[22] Four models (GEOS-CHEM, RAQMS, MOZART and STEM) reported trace gas concentrations along the DC-8 flight tracks. Figures 12–14 provide a comparison of observations and model simulations over eastern North America (30–50°N; 260–320°E) where most intense aircraft sampling was performed. Figure 12 shows observed and modeled mean mixing ratios of $O_3$ and $NO_y$. The four models under consideration deviate from each other and the observations at all altitudes. STEM substantially over estimated $O_3$ in the UT and $NO_y$ in all of the troposphere. RAQMS calculated extremely low $NO_y$ but overpredicted $O_3$ possibly because of an unusually large stratospheric input. Models in general tended to predict lesser variability (Figures 12c and 12d) than observations in large part because of the their greater spatial averaging.

[23] Figure 13 shows model-data comparison for $NO_x$, $HNO_3$, PAN and $HO_2NO_2$ profiles. Except in the case of

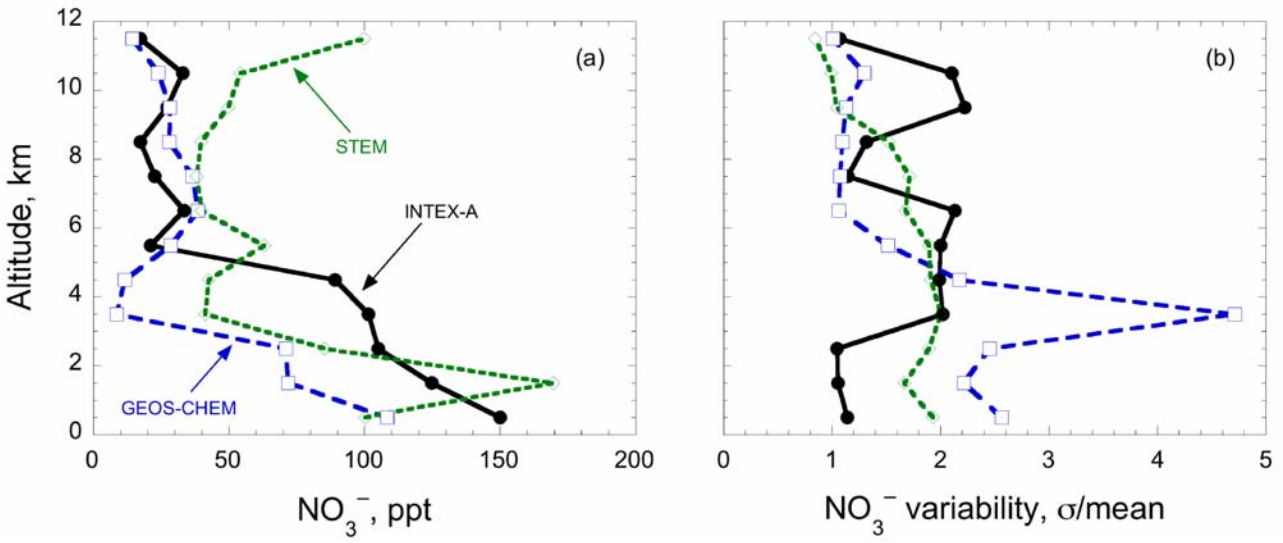


**Figure 14.** Observed and simulated aerosol nitrate concentrations and variability over eastern North America (30–50°N; 260–320°E). Aerosol size cutoff is 5 $\mu$m.

STEM, $NO_x$ was substantially under predicted by all models in the UT. GEOS-CHEM improved its overall prediction by increasing the lightning source over North America by a factor of four [*Hudman et al.*, 2007]. It has recently been suggested that cloud-to-cloud discharges may be a far greater source of $NO_x$ than what has traditionally been believed [*Ridley et al.*, 2005]. An underestimation of the lightning source and uncertainties in its distribution appear to be a common problem in these models. STEM also predicted 50–100% more near surface $NO_x$ and $HNO_3$ than observed. STEM is using an earlier emissions inventory that does not take into account the substantial emission reductions that have recently been achieved most notably by the U.S. power industry. An intriguing aspect is that in the UT, $HNO_3$ is typically over estimated while $NO_x$ is underestimated. As has been noted elsewhere (Ren et al., unpublished manuscript, 2007), models are over calculating OH (and $HO_2$) levels resulting in an over estimation of $HNO_3$ ($NO_2$+OH → $HNO_3$). To simulate $HNO_3$ correctly a significant revision in the $HO_x$ field would be necessary. Thus the observed $NO_x/HNO_3$ ratio provides indirect evidence for the accuracy of the OH measurements during INTEX-A. The situation with PAN (and $HO_2NO_2$) is also confusing with large over estimation by MOZART in the MT and UT and by STEM in the LT. Figure 14 shows the distribution of total aerosol $NO_3$ and its simulation by two models. These models are either able to simulate the UT or LT with reasonable accuracy but not both.

[24] While models have become more complex, it is not clear if the overall performance in simulating reactive nitrogen has improved over the last decade [*Emmons et al.*, 1997; *Thakur et al.*, 1999]. Uncertainties are clearly due to errors in sources and meteorology, but probably include mechanistic limitations in our knowledge. In recent years, it has been possible to retrieve $NO_2$ columns in the troposphere from satellite observations and these have been used to provide extensive data coverage as well as inferences of $NO_x$ emissions [*Richter et al.*, 2005; *Martin et al.*, 2006]. Retrieval of satellite data requires a priori knowledge of $NO_2$ structure and the accuracy of retrievals is often dependent on this knowledge. Traditionally, model profiles have been used for this purpose. The $NO_2$ observations from this study clearly show that the vertical structure of $NO_x$ over continents is highly complex and its extensive characterization is necessary for accurate satellite retrievals.

## 5. Conclusions

[25] INTEX-A provided a detailed description of the reactive nitrogen, ozone, and tracer field in the North American troposphere. The observations clearly showed that the UT as well as LT is significantly polluted across North America. The UT is also more influenced by far greater lightning $NO_x$ emissions than hitherto believed. $NO_x/NO_y$ ratios are significantly more elevated in the UT than in the LT and support fresh injections of $NO_x$ originating in the free troposphere. PAN appears to be the major carrier of reactive nitrogen in the UT while much of it exists in the $HNO_3$ reservoir in the LT. Model simulations of reactive nitrogen species cannot be performed accurately because of uncertainties in lightning sources of $NO_x$ as well as in the $HO_x$ field. Further studies employing all of the improvements in model parameterizations identified as important by comparison to the INTEX-A data will be required to evaluate the extent to which we can now accurately represent the distribution and partitioning of tropospheric $NO_y$ during this period or if there are still other unexplained difference between model and observations.

[26] **Acknowledgments.** We thank all ICARTT participants and sponsoring agencies for making this project possible. DC-8 activities were supported by the NASA Tropospheric Chemistry Program. The National Center for Atmospheric Research is sponsored by the National Science Foundation and operated by the University Corporation for Atmospheric Research.

## References


Bertram, T. H., et al. (2007), Direct measurements of the convective recycling of the upper troposphere, *Science*, doi:10.1126/science.1134548, in press.

Bey, I., et al. (2001), Global modeling of tropospheric chemistry with assimilated meteorology: Model description and evaluation, *J. Geophys. Res.*, *106*, 23,073–23,096.

Brasseur, G. P., et al. (1998), European scientific assessment of the atmospheric effects of aircraft emissions, *Atmos. Environ.*, *32*(13), 2329–2418.

Brown, S. S., et al. (2006), Variability in nocturnal nitrogen oxide processing and its role in regional air quality, *Science*, *311*, 67–70.

Brunner, D., J. Staehelin, D. Jeker, H. Wernli, and U. Schumann (2001), Nitrogen oxides and ozone in the tropopause region of the Northern Hemisphere: Measurements from commercial aircraft in 1995/1996 and 1997, *J. Geophys. Res.*, *106*(D21), 27,673–27,700.

Cleary, P. A., et al. (2005), Observations of total alkyl nitrates within the Sacramento urban plume, *Atmos. Chem. Phys. Disc.*, *5*, 4801–4843.

Cohen, R. C., and J. G. Murphy (2003), Photochemistry of $NO_2$ in Earth's stratosphere: Constraints from observations, *Chem. Rev.*, *103*, 4985–4998.

Cooper, O. R., et al. (2006), Large upper tropospheric ozone enhancements above midlatitude North America during summer: In situ evidence from the IONS and MOZAIC ozone measurement network, *J. Geophys. Res.*, *111*, D24S05, doi:10.1029/2006JD007306.

Crawford, J. H., et al. (1999), Assessment of upper tropospheric $HO_x$ sources over the tropical Pacific based on NASA GTE/PEM data: Net effect on $HO_x$ and other photochemical parameters, *J. Geophys. Res.*, *104*, 16,255–16,273.

Crutzen, P. J. (1979), The role of NO and $NO_2$ in the chemistry of the troposphere and stratosphere, *Annu. Rev. Earth Planet. Sci.*, *7*, 443–472.

Day, D. A., P. J. Wooldridge, M. B. Dillon, J. A. Thornton, and R. C. Cohen (2002), A thermal dissociation laser-induced fluorescence instrument for in situ detection of $NO_2$, peroxy nitrates, alkyl nitrates, and $HNO_3$, *J. Geophys. Res.*, *107*(D6), 4046, doi:10.1029/2001JD000779.

Edwards, D. P., et al. (2004), Observations of carbon monoxide and aerosols from the Terra satellite: Northern Hemisphere variability, *J. Geophys. Res.*, *109*, D24202, doi:10.1029/2004JD004727.

Emmons, L. K., et al. (1997), Climatologies of $NO_x$ and $NO_y$: A comparison of data and models, *Atmos. Environ.*, *31*, 1851–1904.

Fehsenfeld, F. C., et al. (2006), International Consortium for Atmospheric Research on Transport and Transformation (ICARTT): North America to Europe—Overview of the 2004 summer field study, *J. Geophys. Res.*, *111*, D23S01, doi:10.1029/2006JD007829.

Flocke, E., et al. (2005), Results from fast airborne measurements of PANs during the 2004 New England Air Quality Study, *Eos Trans. AGU*, *86*(52), Fall Meet. Suppl., Abstract A54C-03.

Fuelberg, H. E., M. J. Porter, C. M. Kiley, and D. Morse (2007), Meteorological conditions and anomalies during INTEX-NA, *J. Geophys. Res.*, doi:10.1029/2006JD007734, in press.

Holloway, T., H. Levy II, and P. Kasibhatla (2000), Global distribution of carbon monoxide, *J. Geophys. Res.*, *105*(D10), 12,123–12,148.

Horowitz, L. W., et al. (2003), A global simulation of tropospheric ozone and related tracers: Description and evaluation of MOZART, version 2, *J. Geophys. Res.*, *108*(D24), 4784, doi:10.1029/2002JD002853.

Horowitz, L. W., A. M. Fiore, G. Milly, R. C. Cohen, A. Perring, and P. J. Woolridge (2007), Observational constraints on the chemistry of isoprene nitrates over the eastern United States, *J. Geophys. Res.*, doi:10.1029/2006JD007747, in press.

Hudman, R. C., et al. (2007), Surface and lightning sources of nitrogen oxides over the United States: magnitudes, chemical evolution, and outflow?, doi:10.1029/2006JD007912, in press.

Huey, L. G., et al. (2007), Measurement of $HO_2NO_2$ in the upper troposphere during INTEX-NA 2004, *J. Geophys. Res.*, doi:10.1029/2006JD007676, in press.

Huntrieser, H., et al. (2002), Airborne measurements of $NO_x$, tracer species, and small particles during the European lightning nitrogen oxides experiment, *J. Geophys. Res.*, *107*(D11), 4113, doi:10.1029/2000JD000209.

Jaegle, L., D. J. Jacob, Y. Wang, A. J. Weinheimer, B. A. Ridley, T. L. Campos, G. W. Sachse, and D. E. Hagen (1998), Sources and chemistry of $NO_x$ in the upper troposphere over the United States, *Geophys. Res. Lett.*, *25*, 1705–1708.

Koike, M., et al. (2000), Impact of aircraft emissions on reactive nitrogen over the North Atlantic flight corridor region, *J. Geophys. Res.*, *105*(D3), 3665–3677.

Kondo, Y., et al. (1997), Profiles and partitioning of reactive nitrogen over the Pacific Ocean in winter and early spring, *J. Geophys. Res.*, *102*, 28,405–28,424.

Krueger, B. J., V. H. Grassian, J. P. Cowin, and A. Laskin (2004), Heterogeneous chemistry of individual mineral dust particles from different dust source regions: The importance of particle mineralogy, *Atmos. Environ.*, *38*, 6253–6261.

Law, K., et al. (2005), Evidence for long-range transport of North American anthropogenic and wildfire emissions to Europe from airborne and ground based lidar measurements during European ITOP (IGAC Lagrangian 2K4, ICARTT), *Eos Trans. AGU*, *86*(52), Fall Meet. Suppl., Abstract A41D-01.

Martin, R. V., et al. (2006), Evaluation of space-based constraints on global nitrogen oxide emissions with regional aircraft measurements over and downwind of eastern North America, *J. Geophys. Res.*, *111*, D15308, doi:10.1029/2005JD006680.

McNaughton, C. S., et al. (2007), Results from the DC-8 Inlet Characterization Experiment (DICE): Airborne versus surface sampling of mineral dust and sea salt aerosols, *Aerosol Sci. Technol.*, in press.

Miyazaki, Y., et al. (2005), Contribution of particulate nitrate to airborne measurements of total reactive nitrogen, *J. Geophys. Res.*, *110*, D15304, doi:10.1029/2004JD005502.

Perkins, K. K., et al. (2001), The $NO_x$-$HNO_3$ system in the lower stratosphere: Insights from in situ measurements and implications of the $J_{HNO3}$-OH relationship, *J. Phys. Chem.*, *105*, 1521–1528.

Pfister, G., P. G. Hess, L. K. Emmons, J.-F. Lamarque, C. Wiedinmyer, D. P. Edwards, G. Pétron, J. C. Gille, and G. W. Sachse (2005), Quantifying CO emissions from the 2004 Alaskan wildfires using MOPITT CO data, *Geophys. Res. Lett.*, *32*, L11809, doi:10.1029/2005GL022995.

Pierce, R. B., et al. (2003), Regional Air Quality Modeling System (RAQMS) predictions of the tropospheric ozone budget over east Asia, *J. Geophys. Res.*, *108*(D21), 8825, doi:10.1029/2002JD003176.

Pierce, R. B., et al. (2007), Chemical data assimilation based estimates of continental US ozone and nitrogen budgets during INTEX-A, *J. Geophys. Res.*, doi:10.1029/2006JD007722, in press.

Richter, A., J. P. Burrows, H. Nü, C. Granier, and U. Niemeier (2005), Increase in tropospheric nitrogen dioxide over China observed from space, *Nature*, *437*, 129–132.

Ridley, B., et al. (2004), Florida thunderstorms: A faucet of reactive nitrogen to the upper troposphere, *J. Geophys. Res.*, *109*, D17305, doi:10.1029/2004JD004769.

Ridley, B. A., K. E. Pickering, and J. E. Dye (2005), Comments on the parameterization of lightning-produced NO in global chemistry-transport models, *Atmos. Environ.*, *39*, 6184–6187.

Rosen, R. S., E. C. Wood, P. J. Wooldridge, J. A. Thornton, D. A. Day, W. Kuster, E. J. Williams, B. T. Jobson, and R. C. Cohen (2004), Observations of total alkyl nitrates during Texas Air Quality Study 2000: Implications for $O_3$ and alkyl nitrate photochemistry, *J. Geophys. Res.*, *109*, D07303, doi:10.1029/2003JD004227.

Seinfeld, J. H., and S. N. Pandis (1998), *Atmospheric Chemistry and Physics*, John Wiley, Hoboken, N. J.

Singh, H. B., et al. (1996), Reactive nitrogen and ozone relationships over the western Pacific: Distribution, partitioning, and sources, *J. Geophys. Res.*, *101*, 1793–1808.

Singh, H. B., et al. (1997), Trace chemical measurements from the northern midlatitude lowermost stratosphere: Distributions, correlations, and fate, *Geophys. Res. Lett.*, *24*, 127–130.

Singh, H. B., A. M. Thompson, and H. Schlager (1999), SONEX airborne mission and coordinated POLINAT-2 activity: Overview and accomplishments, *Geophys. Res. Lett.*, *26*(20), 3053–3056.

Singh, H. B., W. H. Brune, and J. H. Crawford (2003a), Reactive nitrogen and hydrogen in the global atmosphere: Progress in measurements and theory, in Recent Advances in Atmospheric and Oceanic Sciences Part II: Air Pollution Studies, *Proc. Ind. Natl. Sci. Acad.*, *69/6*, 669–683.

Singh, H. B., et al. (2003b), In situ measurements of HCN and $CH_3CN$ over the Pacific Ocean: Sources, sinks, and budgets, *J. Geophys. Res.*, *108*(D20), 8795, doi:10.1029/2002JD003006.

Singh, H. B., W. H. Brune, J. H. Crawford, D. J. Jacob, and P. B. Russell (2006), Overview of the summer 2004 Intercontinental Chemical Transport Experiment–North America (INTEX-A), *J. Geophys. Res.*, *111*, D24S01, doi:10.1029/2006JD007905.

Tang, Y., et al. (2004), Three-dimensional simulations of inorganic aerosol distributions in east Asia during spring 2001, *J. Geophys. Res.*, *109*, D19S23, doi:10.1029/2003JD004201.

Tang, Y., et al. (2007), The influence of lateral and top boundary conditions on regional air quality prediction: A multi-scale study coupling regional and global chemical transport models, *J. Geophys. Res.*, doi:10.1029/2006JD007515, in press.

Thakur, A. N., H. B. Singh, P. Mariani, Y. Chen, Y. Wang, D. Jacob, G. Brasseur, J.-F. Muller, and M. Lawrence (1999), Distribution of reactive nitrogen species in the remote free troposphere: Data and model comparisons, *Atmos. Environ.*, *33*, 1403–1422.

Wolff, G. T. (1984), On the nature of nitrate in coarse continental aerosols, *Atmos. Environ.*, *18*, 977–981.

Zhao, Y. (2002), Spectroscopic measurements of tropospheric CO, $C_2H_6$, $C_2H_2$, and HCN in northern Japan, *J. Geophys. Res.*, *107*, (D18), 4343, doi:10.1029/2001JD000748.

M. Avery, J. H. Crawford, R. B. Pierce, and G. W. Sachse, NASA Langley Research Center, Hampton, VA 23665, USA.

T. H. Bertram, R. C. Cohen, A. Perring, and P. J. Wooldridge, Department of Chemistry, University of California, Berkeley, CA 92717, USA.

D. R. Blake, Department of Chemistry, University of California, Irvine, CA 92717, USA.

G. R. Carmichael and Y. Tang, Department of Chemical and Biochemical Engineering, University of Iowa, Iowa City, IA 52242, USA.

E. Czech, D. Herlth, R. Kolyer, L. Salas, and H. B. Singh, NASA Ames Research Center, Moffett Field, CA 94035, USA. (eczech@mail.arc.nasa.gov)

J. Dibb, Institute for the Study of Earth, Oceans and Space, University of New Hampshire, Durham, NH 03824, USA.

L. K. Emmons and F. Flocke, National Center for Atmospheric Research, Boulder, CO 80301, USA.

L. W. Horowitz, NOAA Geophysical Fluid Dynamics Laboratory, Princeton, NJ 08542, USA.

R. C. Hudman and S. Turquety, Department of Earth and Planetary Sciences, Harvard University, Cambridge, MA 02138, USA.

G. Huey, School of Earth and Atmospheric Sciences, Georgia Institute of Technology, Atlanta, GA 30332, USA.